Chapter 3

A study of Type II bursts from SMC X-1

.

3.1 Introduction

SMC X-1 is one of the few disc-fed Super Giant X-ray Binaries (SGXBs). Its frequency of pulsation of the pulsar is $\sim$ 1.41 Hz, which is decreasing regularly at the rate of $\sim$ 3.279×10^{-11} Hz s^{-1} (Davison, 1977; Wojdowski *et al.*, 1998). The orbital period of the neutron star around the companion is about $\sim$ 3.9 days. Along with the periodic modulation like pulse period and orbital period the pulsar also show an aperiodic modulation of $\sim$ (55-60) days (Wojdowski *et al.*, 1998). The pulsar shows Type II bursts (Angelini *et al.*, 1991) which are observed as flares in the light curves. There are no abrupt change in the luminosity of the pulsar and softening of the spectrum as a result of the bursts. Moon *et al.* (2003) showed that the flares occupied 3% of the total observational time. The Type II bursts observed in the pulsar and its pulse profiles as well as the change of its spectra due to the bursts are investigated. We have also estimated the total duration of flare and compared

A part of the chapter is published in *Res. Astron. Astrophys.* 18, 148 (2018)

it with the total observational time. The correlation of the flares with time, peak-to-peak ratio of pulse profile, orbital phase and spectral parameters are also explored.

3.2 Observations and Data reduction

The archived RXTE PCA observations of SMC X-1 between 2003-10 and 2003-12 are considered for analysis. As out of the five PCU units of PCA, PCU 0 suffered propane loss in the year 2000, other units namely, PCU 3 and PCU 4 were given rest regularly to avoid break down. However, PCU 2 was operating all the time and did not went through break down. This PCU unit is also best calibrated counter unit which has been verified by fitting the crab spectrum with power law model.

The reduction of data are done using HEASOFT v 6.11. In order to do timing analysis we used *RXTE* PCA data in GOODXENON mode. The GOODXENON data were converted into EVENT mode using the FTOOL *makese*. The light curve of desired binning is then extracted using the FTOOL *seextrct*. Background files are obtained by using STANDARD 2 data and suitable model with the help of FTOOL *runpcabackest*. The background light curve is then extracted from the background files using *saextrct*. The background corrected light curve is then obtained by subtracting the background light curve from the total light curve using the FTOOL *lcmath*. The frame of reference of photon arrival was set to barycentre with the help of *faxbary* using JPL DE400 ephemeries. For our analysis only those data were considered where the elevation of telescope was greater than 10 degree and the data were recorded 30 minutes after the passage of the telescope through South Atlantic anamoly (SAA) region.

For spectral analysis STANDARD 2 *RXTE* PCA data were used which has 129 channels and default binning of 16 s, we have only considered data from top Xe-layer of the PCU 2. In order to obtain response matrix for top layer we used FTOOL *pcarsp*. The background spectrum was extracted from the background file using *saextrct*. The background corrected

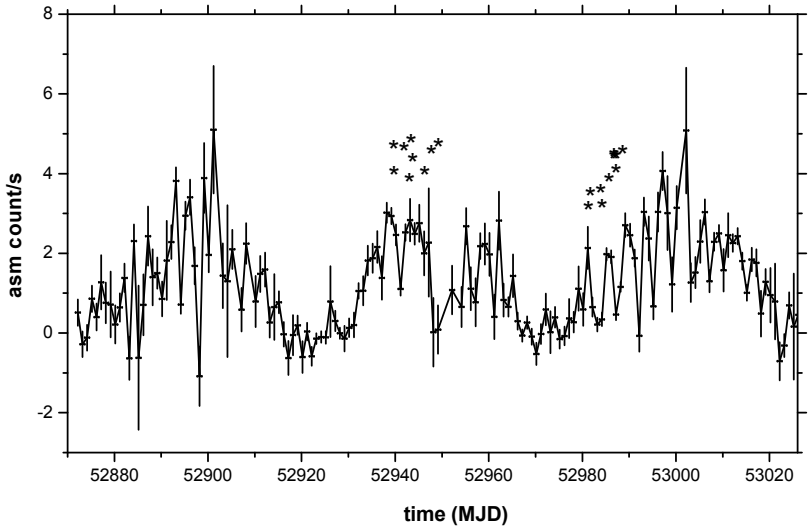

Fig. 3.1 *RXTE* ASM light curve of SMC X-1. The astricks "*" represents the *RXTE* PCA observations. h1 and h2 indicates the high states.

spectrum is obtained by subtracting background spectrum from the total spectrum. Spectra in 3-18 keV energy range were considered for analysis. Spectra above 18 keV were not considered as it is mostly dominated by background and a good fitting not possible. In all the cases a systematic error of 2% have been added to the spectra to cover the uncertainties in the model of the detector response.

3.3 Light curves and flares

SMC X-1 has super-orbital period of ∼55-60 days (Wojdowski *et al.*, 1998), the *RXTE* PCA observations of the pulsar lies in the two high states, h1 and h2 as shown in Fig. 3.1. We have used the method followed by Moon *et al.* (2003) to investigate the flares. Flares were taken as a part of light curves where the photon count rates were 3σ level above the mean. The total data were divided into 110 data segments each of mean duration of 2050 s. Light curve of each data segment was plotted and analyzed.

In order to obtain the duration of bursts we fitted them with a GAUSSIAN model. From the width 'w' of the model we can get FWHM of the burst using $FWHM = 2.35482w$, which we considered as a duration of the burst. The reduced χ^2 of the fitting is found between 2.3-3.56. Initially we started with the light curves having 4 s time resolution and searched for flares, after that we looked for flares in the light curves of 2 s, 6 s and 8 s time resolution. A total of 272 flares have been observed with mean FWHM of $\sim$21 s and standard deviation of $\sim$8 s. So a total of 225.5 ks observational time the source was flaring for 5.7 ks.

Thus the source has undergone through type II bursts for 2.5 % of the time, the value is close to that reported by (Moon *et al.*, 2003). The recurrence time of the flares were observed to vary from few hundreds to thousands of seconds. The average recurrence time between two consecutive flares have been $\sim$ 800 s. The number of flares and the recurrence time are found to be consistent for the light curves of 2 s, 6 s and 8 s time resolutions. The power spectra of the X-ray pulsar are obtained by Fourier transformation of 0.075s time resolution using XRONOS tool *powspec* with normalization=-2. This value of normalization gives us the white noise subtracted normalised power spectra whose integral is related to the r.m.s fractional variability. The r.m.s variability of the four light curves obtained from the power spectra were (a) 30.86%, (b) 31.2 %, (c) 31.2 % and (d) 30%. The source was equally variable in all the four cases. The sharp peak at $\sim$ 1.41 Hz corresponds to the pulse frequency, the other peaks represent the harmonic components (See lower panel of Fig. 3.2).

Large flares where count rate reached few times above the mean have been observed, where in some cases flares had duration of hundreds of seconds. In Fig. 3.3 (*left*) a flare of almost $\sim$ 50 s is shown having two peaks. The first peak arises due to sharp rise in the count rate from the mean value of $\sim$ 300 counts s^{-1} reaching a maximum of $\sim$ 1350 counts s^{-1}. After that count rate falls sharply to $\sim$ 510 counts s^{-1}, followed by sharp increase

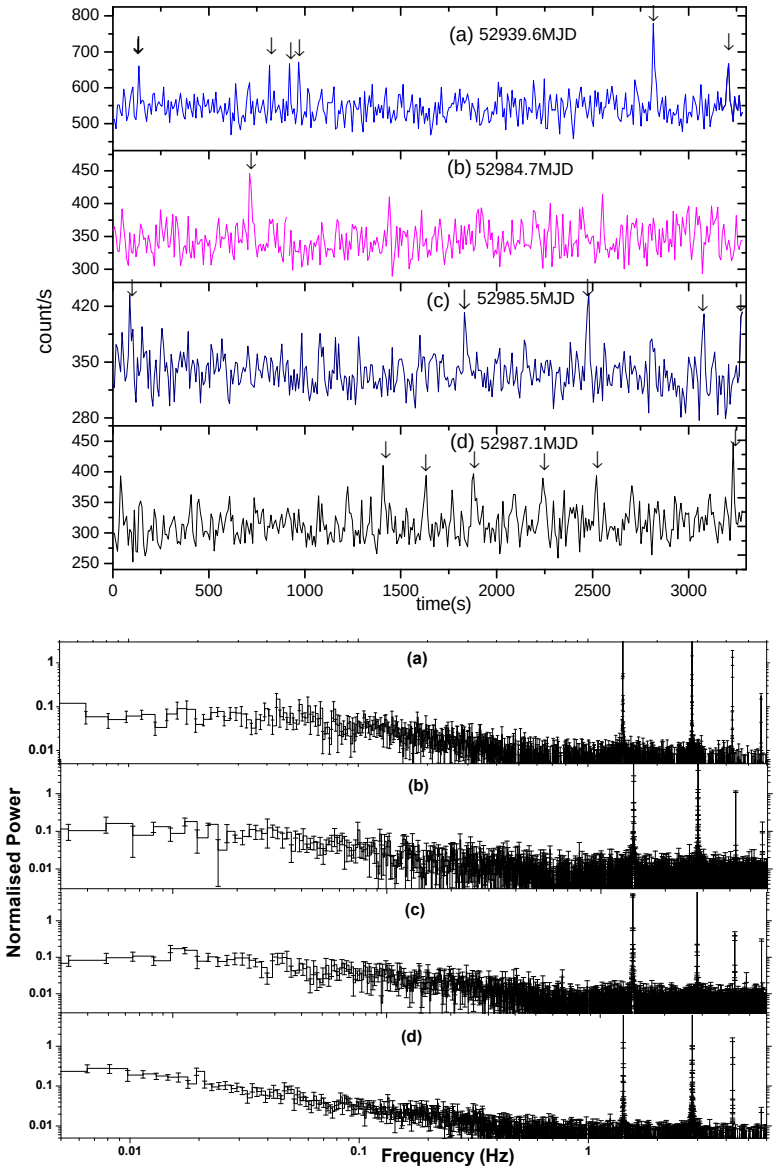

Fig. 3.2 *Upper panel* - Light curves for four different *RXTE*-PCA observations. The down arrow represent flares. *Lower panel* - Power density spectrum for the corresponding light curves.

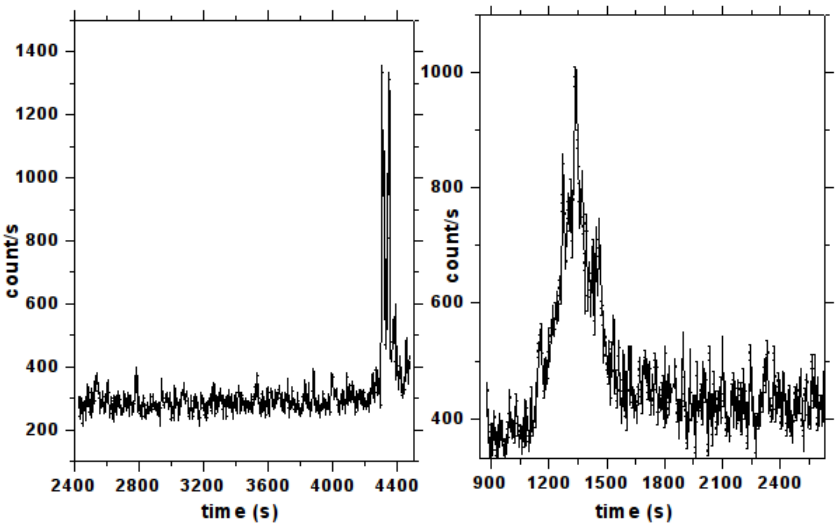

Fig. 3.3 *Left* - Sharp burst observed in SMC X-1. *Right* - Large flare having duration $\sim$ 300 s. These two large flares are from *RXTE* observation having Obs Id 80078-01-01-04.

in count rate giving a second peak of $\sim$ 1320 counts s^{-1} which falls below $\sim$ 500 counts s^{-1}. On the right of the Fig. 3.3 flares having duration of $\sim$ 300 s and accompanying of multiple peaks are found to exist, the highest peak being of $\sim$ 1000 counts s^{-1}. The average number of flares observed per hour in h1 state is 5 and in h2 state is 4 with the average time between two flare being $\sim$ 800 s.

3.4 Pulse profiles

A pulse profile is obtained by folding the light curve of the X-ray pulsar about $\sim$ 0.7 s. As the neutron star moves in a binary orbit there will be delay in pulse arrival time due to orbital modulation *i.e.* when the neutron star is facing the observer the pulse will arrive sooner than when it is away from the observer. So in order to get the correct pulse profile the pulse arrival time of the pulse must be corrected for orbital modulation. The binary orbit of SMC X-1 is almost circular (Levine *et al.*, 1993; Raichur and Paul, 2010; Wojdowski *et al.*, 1998). Let t'_n and t_n be the emission and arrival time of the pulse respectively, which

are related with the each other and the neutron star orbital parameters through the following relations,

$$t_n' = t_0 + nP_s + \frac{1}{2}n^2\dot{P}_sP_s$$
$$t_n = t_n' + f_{orb}(t_n')$$

where P_s and $\dot{P}_s$ are the spin period and its time derivative respectively. For circular orbit $f_{orb}(t_n')$ is given by,

$$f_{orb} = a_x \, sin \, i \, cos \, l_n,$$
$$l_n = 2\pi\frac{(t_n' - E)}{P_{orb}} + \frac{\pi}{2}$$

where l_n is known as the mean orbital longitude at time t_n' and E is the epoch when the mean orbital longitude is $\pi/2$, $a \, sin \, i$ is the projected semi-major axis and i is the angle of inclination between the orbital angular momentum vector and the line of sight. The value of the epochs and the other orbital parameters are used from Raichur and Paul (2010). The orbital corrected pulse profiles is shown in Fig. 3.4. The pulse fractions for (a) and (d) is about 20% and for (b) and (c) 30%. It is observed that the secondary peaks of the pulse profile is found to coincide with each other. Except the change in the height of the primary peak and the pulse fraction, there is no significant change in the shape of the pulse profiles.

3.5 Hardness ratio

In order to estimate the hardness ratio we divided the 7-16 keV light curve by 3-7 keV light curve. The hardness ratio for the four observations (a), (b), (c) and (d) are shown in Fig. 3.5. The average values of hardness ratio for the four observations were 0.90, 0.897,

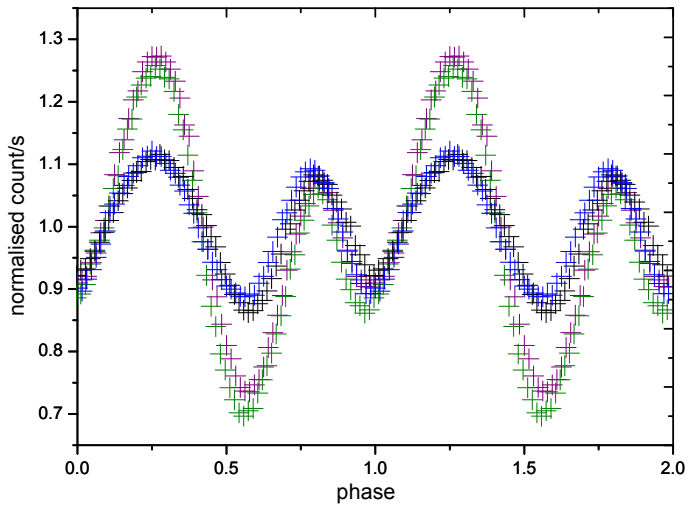

Fig. 3.4 Orbital corrected pulse profiles for four light curves (a), (b), (c) and (d) represented by blue, purple, green and black respectively.

0.856 and 0.837 respectively. No significant change in the hardness ratios are observed in the four light curves during the bursts. Thus the hardness ratio cannot be correlated with flares. We can check these invariance in the hardness ratios by studying the energy spectra of the source.

3.6 Spectral analysis

The energy spectra in 3-18 keV energy range were fitted with PHABS, POWERLAW, HIGHECUT and GAUSSIAN models. The PHABS model is used to estimate the photo-electric absorption of photons by an interstellar medium. The non-thermal emission of the source is estimate by HIGHECUT model, where as the GAUSSIAN model was used to estimate the iron emission line energy. The emission line energy of GAUSSIAN model was fixed at 6.7 keV. The best fitted spectral parameters are shown in Table 3.1

None of the spectral parameters are found to vary significantly for the four spectra. Considering the distance to the SMC X-1 equal to 65 kpc (Keller and Wood, 2006) the

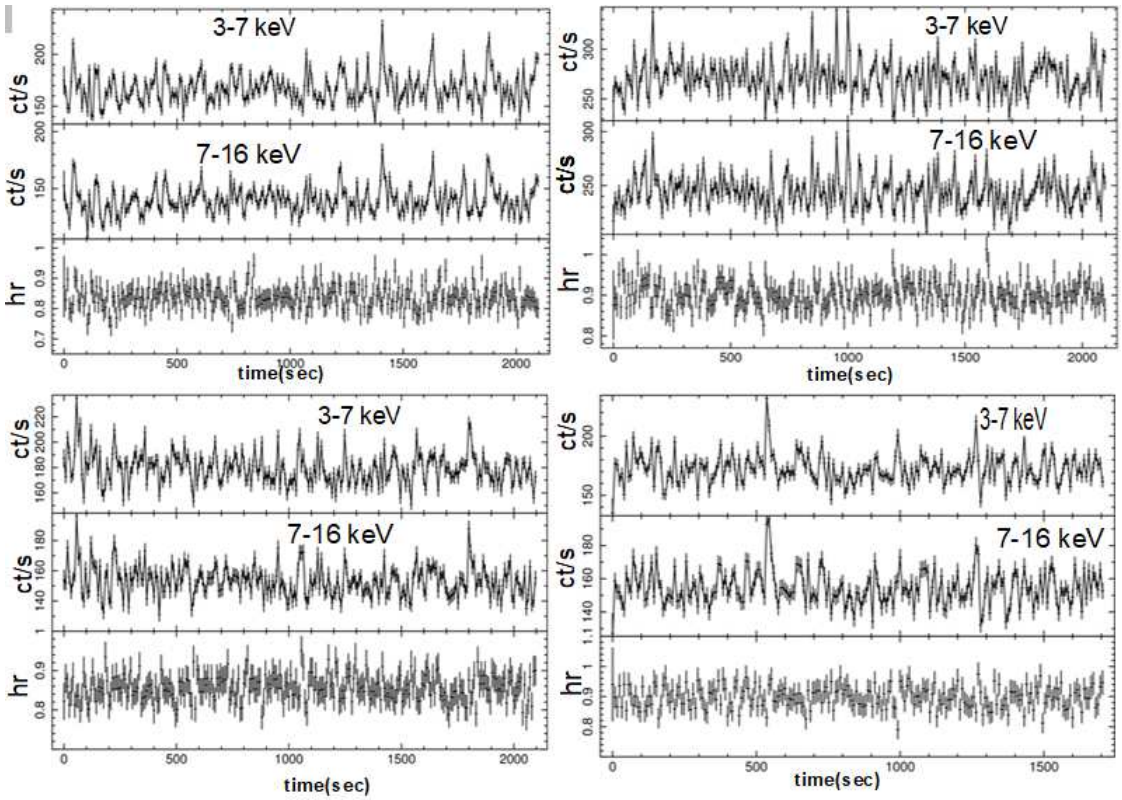

Fig. 3.5 Hardness ratio obtained by dividing the 7-16 keV X-ray count rates by 3-7 keV count rates for four different observations.

observations	a	b	c	d
n_H (10^{22} cm^{-2})	2.062±1.023	1.014±1.06	1.604±1.043	1.968±1.019
α	1.066±0.202	1.004±0.219	1.084±0.218	1.122±0.202
E_{fold} (keV)	17.868±4.726	16.521±4.457	17.723±5.078	17.080±4.143
E_{cutoff} (keV)	5.998±1.045	5.870±1.074	5.837±1.147	6.002±1.218
$flux$ (10^{-9} erg cm^{-2} s^{-1})	1.345	1.247	1.229	1.160
χ^2_ν	1.682	1.375	1.890	1.563

Table 3.1 Table showing best fitted spectral parameters for four spectra. χ^2_ν is the reduced chi-square for 29 dof. n_H is the hydrogen column density and α is the photon-index of POWERLAW model. E_{cutoff} and E_{fold} are the cutoff energy and e-folding energy of the HIGHECUT model *respectively*.

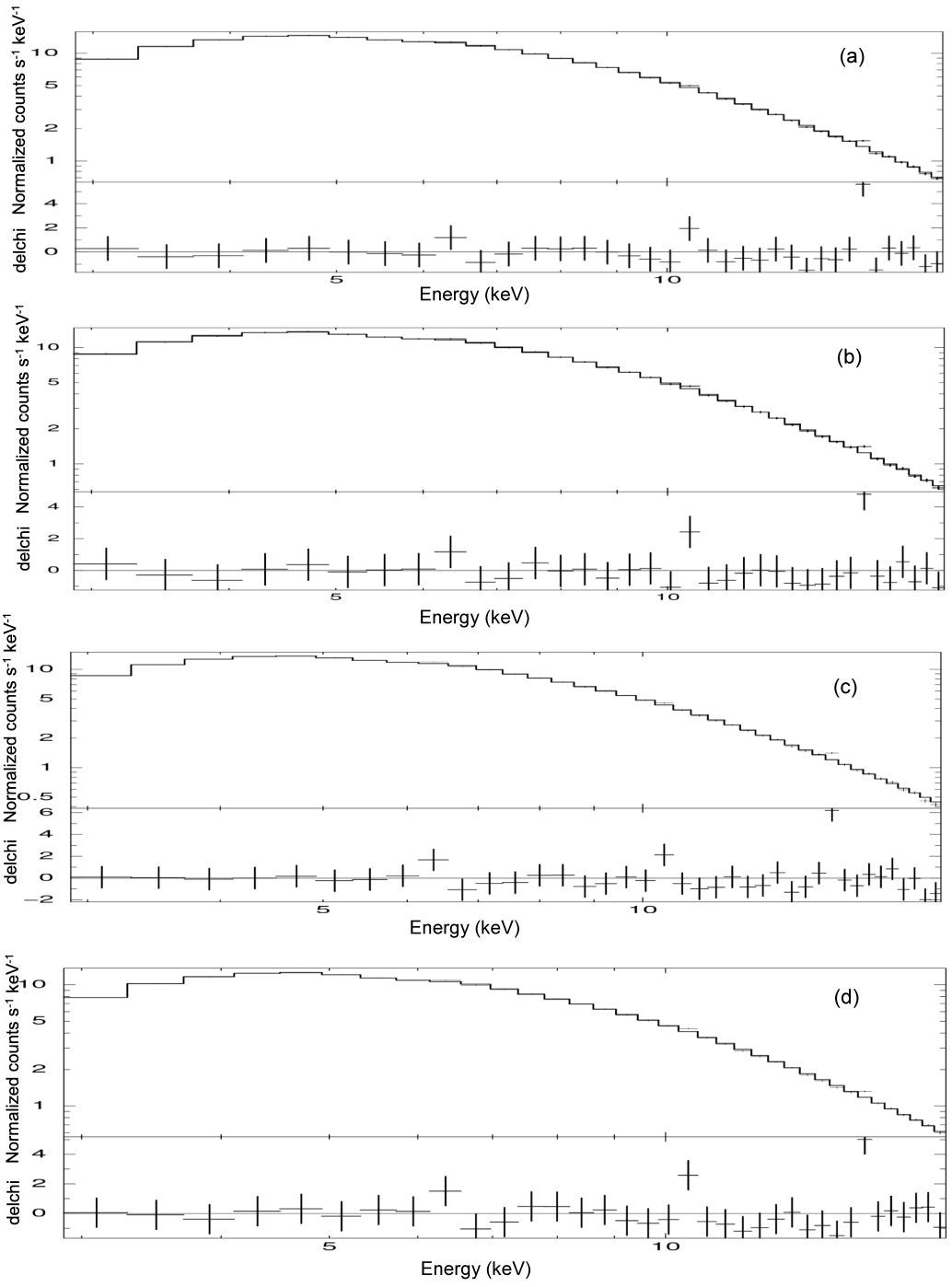

Fig. 3.6 The best fitted spectra for four *RXTE*-PCA spectra in 3-18 keV energy range.

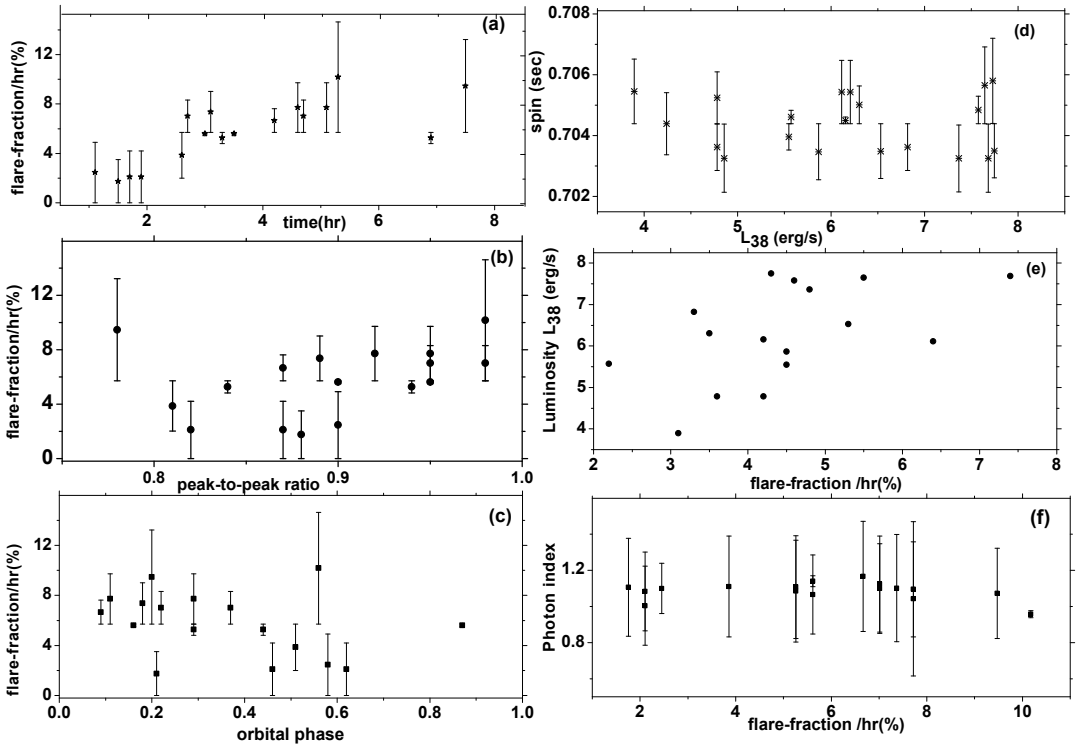

Fig. 3.7 The variation of the flare fraction with the observation time is given by panel figure in panel (a), where as variation of flare-fraction with peak-to-peak ratio and orbital phase are given by figures (b) and (c) respectively. Figure (d) shows the variation of spin with the luminosity where as figure (e) is luminosity of different observations plotted against flare-fraction. Figure (f) is the variation of the photon index with the flare-fraction.

luminosity of the four observations are estimated to be 6.787×10^{38} erg s^{-1}, 6.302×10^{38} erg s^{-1}, 6.211×10^{38} erg s^{-1} and 5.862×10^{38} erg s^{-1} respectively. The variation of the column density may be a result of partial obscuration of the neutron star due to the precessing accretion disk or due to X-ray eclipses. The photoelectric absorption being dominated in the soft energy range but as we cannot go below 3 keV energy due to the limitation of the instrument, so its not possible to constrain the value of column density exactly.

3.7 Variation of flare-fraction with observational time, pulse peak-to-peak ratio and orbital phase

It is evident from the Fig. 3.7a that the flare-fraction increases with the increase in the observational time. The flare fraction is defined as the ratio of number of flares present in particular observation to the total number of flares divided by the observational time which is expressed in % hr^{-1}. The peak to peak ratio is defined as the ratio of secondary to primary peak. As it is clear from the Fig. 3.7b the flare fraction increases with an increase in the pulse peak to peak ratio. The flare-fraction is high in the orbital phases between 0.0-0.45 and then it decreases (Fig 3.7c). The variation of the flare fraction can be as a result of change in accretion rate which affects the number of bursts observed. The pulse period of the X-ray pulsar is dependent on the luminosity, so in order to study the variation of the pulse period with the luminosity we plotted the pulse period (spin) with the luminosity (Fig. 3.7d). To observe the change in the spectral properties with the flare we plot the variation of the photon index with the flare fraction (Fig.3.7f) for different observations. No correlation of the flare fraction with the photon index is observed. A little bit of hardening of the spectrum is observed when the flare fraction is $\sim$10 %. As no clear correlation can be set between the flare fraction and the small hardening of the spectrum it may be due to decrease in the photoelectric absorption by the interstellar medium and not due to increase in flare fraction. Also it is evident from the Fig 3.7e the luminosity is found to increase with the increase in flare fraction. So strong positive correlation of the luminosity with the flare fraction is observed here.

The spin period for a given observation is obtained from the orbital corrected light curves using EFSEARCH. The spin period in our observations lies between 0.7033 to 0.707 s, where as the luminosity lies between 3.9-7.8$\times 10^{38}$ erg s^{-1}. Theoretically the spin-up rate ($\dot{P}$) of the X-ray pulsars is found to be proportional to $PL_{38}^{3/2}$ (Ghosh and Lamb, 1979),

where P is the spin period of the neutron star and L_{38} is the luminosity of the pulsar in the order of 10^{38} erg. The SMC X-1 shows secular spin-up and the spin-up rate ($\dot{P}$) which is about 3.279×10^{-11} Hz s^{-1} (Davison, 1977; Wojdowski *et al.*, 1998). As the separation between the two high states is about 50 days so there will be a negligible spin-up. Hence in this case $PL_{38}^{3/2}$ is a constant *i.e.* $P \propto L_{38}^{-3/2}$. No such variation of the spin with the luminosity is observed as it can be due to the fact that the data considered here are from the observations taken over few months. So it might be possible to study the dependence of the spin on the luminosity for SMC X-1 considering long term observations covering few decades using different mission. However this study is complicated due to superorbital modulation of luminosity due to which the luminosity varies in an aperiodic manner.

3.8 Variation of the spectral parameter with orbital phases and flux

In order to study the variations of different spectral parameters with the orbital phase we have fitted the spectra of different *RXTE* PCA observations taken in different orbital phases. The spectra in 3-18 keV energy range were fitted with the models used above. The variation of the photon index (α), column density (n_H) and flux are shown on the left of Fig. 3.8. As it is evident from the figure no abrupt change in the photon index and column density with the orbital phase are observed. The spectral flux (Fig. 3.8c) is observed to vary significantly with the orbital phase that lies between 9.92×10^{-10} to 1.73×10^{-9} erg cm^{-2} s^{-1}. The maximum value of the flux occurs at phase 0.44 and minimum occurs at 0.16. When the flux is maximum then the value of n_H is minimum which is about 1.02×10^{22} cm^{-2}. From figs. 3.8(a), 3.8(c) and 3.8(d) we found that at the orbital phase 0.17 the spectrum is a bit softer with the maximum value of the photon index 1.12 along with the maximum value of n_H is $\sim2.42\times10^{22}$ cm^{-2}. Also the hardening of spectrum is

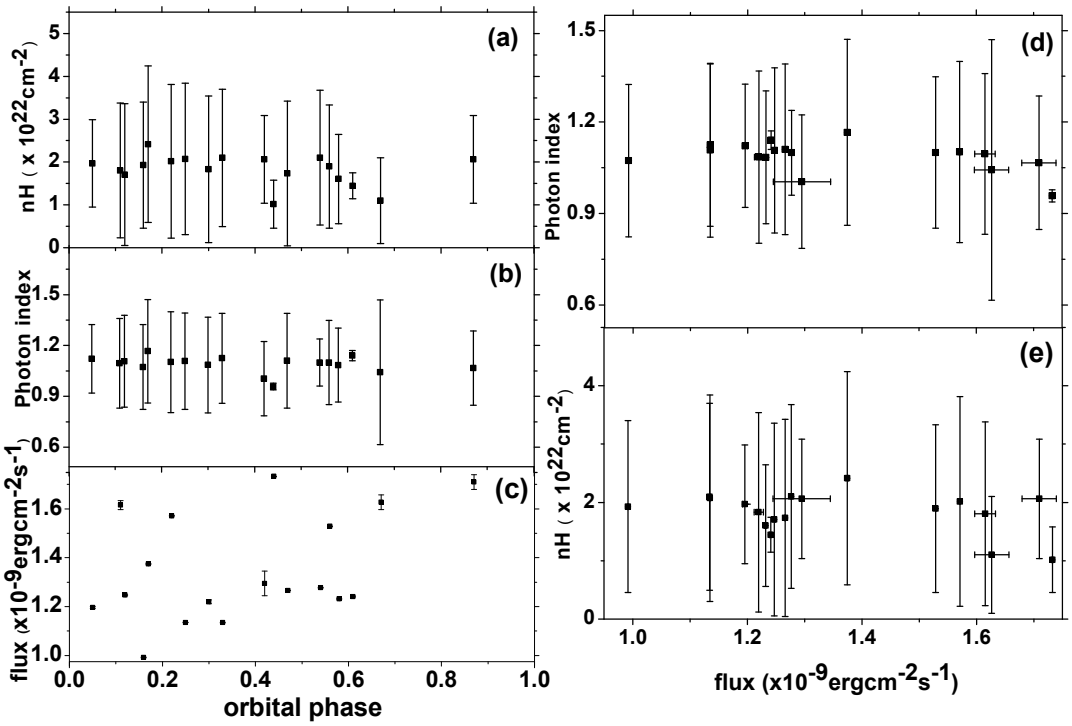

Fig. 3.8 (a), (b) and (c) represents the variation of column density, photon index and flux respectively.

seen when the flux is maximum with photon index 0.96. No clear softening or hardening of the spectra with flux is observed. When the hydrogen column density was minimum the spectrum was a bit harder which can be due to low absorption of hard X-rays in the interstellar medium and it results in maximum flux observed at that phase. In the same way a small softening of the spectra can be as a result of increase in absorption of X-ray by interstellar medium. The variation of flux with the orbital phases may be due to an increase in mass accretion rate.

3.9 Discussion

SMC X-1 exhibits series of type II bursts. The mean recurrence time of the burst was $\sim$ 800 s and almost covers 2.5% of total observing time. The average number of burst per

hour was about 4-5. The type II bursts differs from the type I burst in shape. The type I bursts have sharp rise and falls slowly and gradually in exponential manner where as the type II bursts are recognized by sharp increase and decrease in the count rates in the light curves. Also the origin of the type I burst is due to unstable thermonuclear burning of accreted matter on the surface of the neutron star, where as type II burst are due to increase in accretion rate. During the type I bursts the luminosities of the X-ray pulsars can reach about 10^{39} erg s^{-1} in few seconds. The type II bursts are thought to be due to Lightman-Eardley instability that developed in the accretion disk. No abrupt change in the luminosity is observed during the type II burst.

Short bursts of few seconds to long burst of few hundreds of seconds are observed study of SMC X-1. The shape of the pulse profiles were almost same for different observations which suggest that the geometry of the accretion disk is unchanged due to bursts. The ratio of the secondary to primary peaks of the pulse profile is found to increase with the increase in flare fraction, which may be due to an increase in the accretion rate along the fainter or colder pole of the neutron star during bursts (Moon *et al.*, 2003). With an increase in accretion rate there is an increase in flare fraction. Accretion of nearly same amount of matter on to the two poles of the neutron star may be the cause for the primary and secondary peak of being nearly of same height. With the increase in the flare fraction the luminosity is found to increase, which can be due to increase in the rate of conversion of accreted matter into radiation.

When the radiation pressure dominates over the total pressure in the inner radius of the accretion disk the Lightman-Eardley instability occurs. The instability will trigger the thermal as well as the surface density instability. The investigation on the global nature of the instability were done by Taam and Li (1984) and Lasota and Pelat (1991) and found that the instability leads to burst with recurrence time of few seconds which are similar to that of the three outburst observed in GRO J1744-28 during 1996 (Cannizzo, 1996),

having duration of $\sim$ 10 s and recurrence time of $\sim$ 1000 s. According to Cannizzo (1996) the fast recurrence of the bursts seen by Taam and Li (1984) and Lasota and Pelat (1991) where due to a given value of the viscosity parameter 'α' (Shakura and Sunyaev, 1973), which they set equal to 1 and considered the inner radius (r_{inner}) to be equal to the radius of the neutron star. For burst to occur in GRO J1744-28 the accretion rate must be slightly greater than the critical value such the radiation pressure becomes comparable to the gas pressure. Taking the value of α less than 1 and r_{inner} greater than the radius of the neutron star, the viscous timescale at the critical condition is found to be $t_{\nu,crit} = 1200\, r_8^{0.58} m^{0.79}$ s, where r_8 is the inner radius in the order of 10^8 cm, m is the mass of the neutron star in the order of solar mass ($M_\odot$). Taking the value of $r_{inner} = 10^{7.5}$ cm and $m = 1$ (Cannizzo, 1996) we get $t_{\nu,crit} \sim 800$ s, which is in good agreement with the recurrence time observed in the burst of GRO J1744-28.

The burst from SMC X-1 is similar to that one observed in GRO J1744-28 but the post-flare dip is absent in the former source. Dips in the GRO J1744-28 are observed after the burst and it is thought to be due to depletion of accreted matter after the burst. The absence of dips in SMC X-1 may be due to slow accumulation of matter after a burst or due to release of energy from small fraction of accumulated matter during the burst such that the intensity is found in the persistent level. Another possible reason for the absence of dips may be an increase in the accretion rate just after the burst.

In the source taken here no correlation of the flare-fraction/hr, column density (n_H) and flux with the orbital phase are found. We do not find any change in the nature of the spectrum due to flares. The small softening or hardening of the spectrum can be due to varying interstellar absorption. The SMC X-1 and GRO J1744-28 shows similar spectral properties, as in the case of GRO J1744-28 there is no spectral softening observed in SMC X-1. The spectrum of both sources are inconsistent with the blackbody, the spectrum of GRO J1744-28 photon index 1.2 with the high cutoff energy of 14 keV (Sazonov *et al.*,

1996). Thus burst in these two X-ray binaries are of the same type and can be due to LE instability.

Due to the low magnetic field of the pulsar the transition region between the radiation dominated region and gas pressure dominated region is located near the inner edge of the disk (Li and van den Heuvel, 1997), such that the instability developed inside the disk cannot propagate any further resulting in the heating of matter because of increase in the viscosity. The heated matter is then accreted onto the neutron star producing short burst. The viscosity parameter (α) in the transition region between the radiation dominated and gas pressure dominated region is given by $\alpha = 216\ \frac{\dot{M}_{17}}{t_{visc}^{3/2}}$, where $\dot{M}_{17}$ is the rate of accretion in the order of 10^{17}, t_{visc} is the viscous time scale. The viscous parameter can be estimated by taking the value of $\dot{M}_{17} = 20$ gm s^{-1} and $t_{visc} = 800$ s which is $\alpha \sim 0.16$. Considering the recurrence time of the burst to be equal to the viscous time scale we will get $\alpha \sim 0.16$. A huge accumulation of matter in short time may cause large burst in short time where as if the accumulation of matter takes place slowly causing an instability to develop in a large area for a long time can results in long burst of multiple peaks.